Metals **2015**, *5*, 1188-1196; doi:10.3390/met5031188

OPEN ACCESS

metals

ISSN 2075-4701

www.mdpi.com/journal/metals/

Article

The Self-Organized Critical Behavior in Pd-based Bulk Metallic Glass

Zhong Wang [1], Jiaojiao Li [1], Wei Zhang [2], Junwei Qiao [1,3,*] and Baocheng Wang [1,*]

[1] Laboratory of Applied Physics and Mechanics of Advanced Materials, College of Materials Science and Engineering, Taiyuan University of Technology, Taiyuan 030024, China; E-Mails: wangzhong201209@gmail.com (Z.W.); lijiaojiao1004@gmail.com (J.L.)

[2] School of Materials Science and Engineering, Dalian University of Technology, Dalian 116024, China; E-Mail: wzhang@dlut.edu.cn

[3] Key Laboratory of Interface Science and Engineering in Advanced Materials, Ministry of Education, Taiyuan University of Technology, Taiyuan 030024, China

***** Authors to whom correspondence should be addressed; E-Mails: qiaojunwei@gmail.com (J.Q.); w-baocheng@163.com (B.W.); Tel.: +86-351-6018-051 (J.Q. & B.W.); Fax: +86-351-6010-311 (J.Q. & B.W.).

Academic Editor: Yong Zhang

Received: 25 May 2015 / Accepted: 25 June 2015 / Published: 6 July 2015

Abstract: Bulk metallic glasses (BMGs) deform irreversibly through shear banding manifested as serrated-flow behavior during compressive tests. The strain-rate-dependent plasticity under uniaxial compression at the strain rates of 2×10^{-2}, 2×10^{-3}, and 2×10^{-4} s^{-1} in a Pd-based BMG is investigated. The serrated flow behavior is not observed in the stress-strain curve at the strain rate of 2×10^{-2} s^{-1}. However, the medial state occurs at the strain rates of 2×10^{-3} s^{-1}, and eventually the self-organized critical (SOC) behavior appears at the strain rate of 2×10^{-4} s^{-1}. The distribution of the elastic energy density shows a power-law distribution with the power-law exponent of −2.76, suggesting that the SOC behavior appears. In addition, the cumulative probability is well approximated by a power-law distribution function with the power-law exponent of 0.22 at the strain rate of 2×10^{-4} s^{-1}. The values of the goodness of fit are 0.95 and 0.99 at the strain rates of 2×10^{-3} and 2×10^{-4} s^{-1}, respectively. The transition of the dynamic serrated flows of BMGs is from non-serrated flow to an intermediate state and finally to the SOC state with decreasing the strain rates.

Keywords: bulk metallic glass; serrated flow; plasticity; self-organized critical behavior

1. Introduction

Bulk metallic glasses (BMGs) have attracted significant scientific and technological attention, since they exhibit extraordinarily high strengths about two times or even higher than that of their crystalline counterparts at ambient temperature, due to the absence of dislocations [1,2]. However, their use as structural materials is severely limited because of their poor ductility and catastrophic failure at room temperature arising from the shear localization [3,4]. Lack of long-range atomic order, the underlying deformation mechanisms of BMGs are completely different from the crystalline alloys. Several theoretical models including the free volume [5], shear-transformation zone (STZ) theory [6], and cooperative shear model (CSM) [7] have been proposed, providing a comprehensive description to the plasticity of BMGs. Despite the success of these theories in revealing the fundamental flow process, demonstrating the macroscopic plastic deformation behavior with these microscopic theories still keeps some challenges in BMGs.

The discontinuous yielding in crystalline alloys is well known to exhibit temporal fluctuations during plastic deformation on the stress-strain curves [8]. These fluctuations are accompanied by the spatial localization of dislocations into narrow bands [9], which are called the Portevin-Le Chatelier (PLC) effect [10]. The physical origin of the intermittent flows is attributed to the collective movement of dislocations [11]. The plastic deformation is a complex inhomogeneous process in the crystalline solids, and the dislocation motions are characterized by scale-free and intermittent avalanches [12], which are reminiscent of the concept of self-organized critical behavior (SOC) [13]. The SOC behavior is characterized by the continuous propagation of deformation bands near the upper strain rate boundary of plastic instability [14]. Although dislocation-mediated deformation mechanisms are absent in BMGs, the serrated flow phenomenon has been widely observed in compressive tests [15–17], which is associated with shear-band formation and propagation [18]. Wang *et al.* [19] suggested that the artificial external disturbance of plastic instability to enhance SOC behavior can effectively improve the ductility of BMGs. Sun *et al.* [20] showed that the plastic deformation of ductile BMGs can evolve into a SOC state characterized by the power-law distribution of shear avalanches. Ren *et al.* [14] found that the plastic dynamics of BMGs transition from a chaotic state to the SOC state are correlated with increasing strain rates and decreasing temperatures. In order to explore the serration dynamics in a Pd-based BMG, the amplitudes of serrations, compressive plasticity, as well as the SOC behavior of $Pd_{75}Si_{15}Ag_3Cu_7$ BMGs at different strain rates during serrated flows are investigated by statistical dynamical analysis.

2. Experimental Procedures

Alloy ingots with a nominal composition of $Pd_{75}Si_{15}Ag_3Cu_7$ [21] were prepared by arc-melting a mixture of pure metals (weight purity $\geq$ 99.9%) in a Ti-gettered argon atmosphere. To ensure the compositional homogeneity, each ingot was remelted at least four times. Rod-shaped samples with a diameter of 2 mm and a length of about 60 mm were prepared by suction casting into a water-cooled copper mold. Compressive testing specimens about 4 mm long were cut from the rod-like samples by

a diamond saw with the cooling water, and then, carefully polished with an aspect ratio (height:diameter) of 2:1 to an accuracy of 5 μm. The uniaxial-compressive tests were conducted at the strain rates of 2×10^{-2}, 2×10^{-3}, and 2×10^{-4} s^{-1} at 298 K (room temperature) on the cylindrical specimens using a MTS 809 materials-testing machine (Meitesi Industry System, Minneapolis, MN, USA). The fracture surface of the specimens was observed using the scanning-electron microscopy (SEM, Tescan, Brno, Czech) to identify fracture mechanisms.

3. Results and Discussion

The $Pd_{75}Si_{15}Ag_3Cu_7$ BMG exhibits only one major exothermic event, indicating that this alloy is located near a Pd–Si–Ag–Cu eutectic point, which means that the high glass formation ability occurs and the critical diameter is 10 mm [21]. Meanwhile, this Pd-based BMG possesses good mechanical properties, including the compressive yielding strength of 1608 MPa, Yong's modulus of 100 GPa, and plastic strain of 4.4% [21], as displayed in Figure 1. The compressive engineering stress-strain curves of the $Pd_{75}Si_{15}Ag_3Cu_7$ BMGs exhibit serrated flow behavior after yielding at different strain rates of 2×10^{-2}, 2×10^{-3}, and 2×10^{-4} s^{-1} at ambient temperature, which are shown in Figure 1a. The yielding point is regarded as that when the first serration appears on the stress-strain curve [22]. It is obvious that the yielding strengths are almost the same value of 1650 MPa, and the compressive plasticity keeps similar values about ~6% at different strain rates. The repeating cycles of a sudden stress drop are followed by reloading elastically, which accord with the previous results [23–25]. In order to eliminate the machine vibration error, any serration event with a stress fluctuation less than 5 MPa in jerky flows is excluded in the present statistical analysis. When the strain rate is 2×10^{-2} s^{-1}, the number of the serrations is 9, and most of the amplitudes of these serrations are lower than 5 MPa, as displayed in the inset of Figure 1a. These small serrations are induced by a vibration resulting from the motion of the cross-heads in the machine [19,23]. In this case, although the serrations occur on the stress-strain curve, it is treated as non-serrated-flow behavior at the strain rate of 2×10^{-2} s^{-1}, which is not discussed in the current research. In contrast, it is clear that the serrated-flow phenomena are evident on the stress-strain curves at the strain rates of 2×10^{-3} and 2×10^{-4} s^{-1}, as shown in Figure 1b,c, respectively. In this study, all the serrations are counted in this study at different strain rates of 2×10^{-3} and 2×10^{-4} s^{-1}. Based on the transformation between the strain energy and heat, Qiao *et al.* [26] have proposed a model to predict the amplitudes of the serration events by $\Delta\sigma=\sqrt{\left[2l_vE\rho c_p\left(0.8T_g-T_r\right)\right]/0.9aD\sin\theta}$, where l_v is the thickness of the shearing layer, E is the Young modulus of the BMG, ρ is the density, c_p is the heat capacity, T_g is the glass-transition temperature, T_r is the room temperature with a value of about 298 K, a is the aspect ratio ($a = H/D$), D is the diameter, and θ is the shear angle. The predicted maximum value of the amplitude of serration is 69 MPa, and the average amplitudes of serrated flows are 28 and 22 MPa at the strain rates of 2×10^{-3} and 2×10^{-4} s^{-1} in this study, respectively, which is in the same order of magnitude.

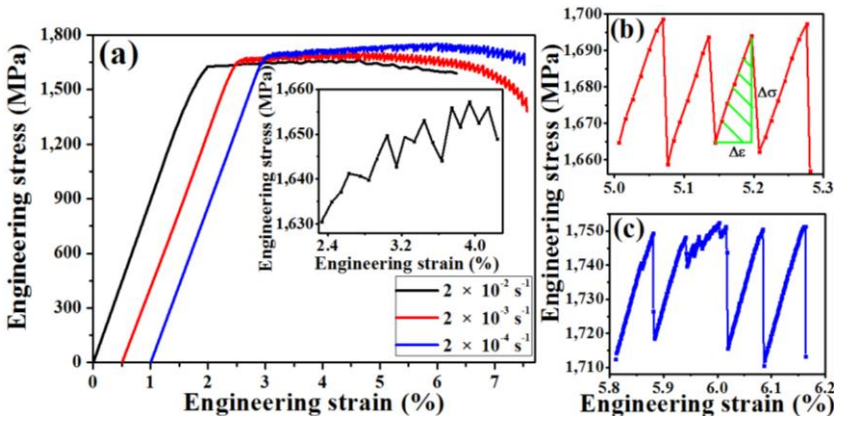

Figure 1. (**a**) Engineering stress-strain curves of the $Pd_{75}Si_{15}Ag_3Cu_7$ bulk metallic glass (BMG) compressed at three strain rates. Inset shows the local engineering stress-strain curve at the strain rate of 2×10^{-2} s^{-1}. (**b**,**c**) Serration events are selected randomly at the strain rates of 2×10^{-3} and 2×10^{-4} s^{-1}, respectively.

The deformation morphologies of the samples at different strain rates are observed by SEM to reveal the dynamic serrated-flow behavior and fracture mechanism. Figure 2a,b are the enlarged profiles of the lateral surfaces, indicated in the dashed rectangles in each inset at the strain rates of 2×10^{-3} and 2×10^{-4} s^{-1}, respectively. The whole fracture photographs of the corresponding deformed samples are displayed in the insets of Figure 2a,b, respectively. It is obvious that the fractured BMGs present a shear fracture mode with a shear angle about 43 degrees with respect to the loading direction in Figure 2a. Many shear bands can be captured and the formation of micro-cracks occurs through multi-step shearing by energy dissipation of shear banding [23], as exhibited by the arrows. In Figure 2b, profuse shear bands can be found on the surface and the shear bands display an intensive arrangement. Some secondary shear bands propagate along different directions. It is suggested that shear banding is the main mechanism dominating the dynamics of serrated flows.

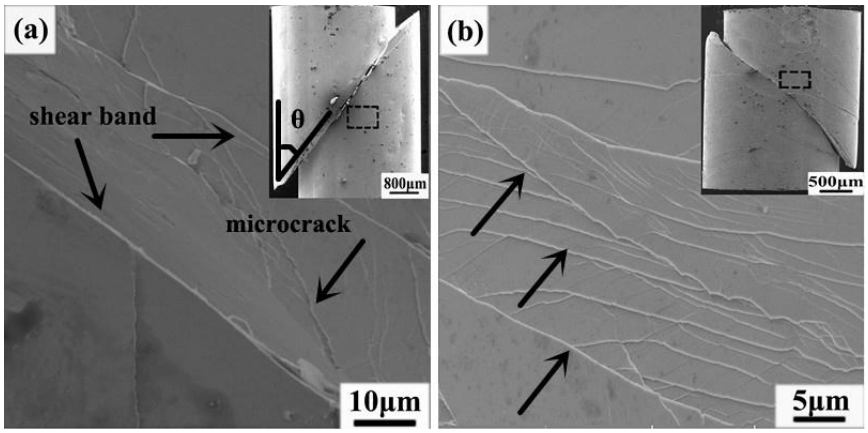

Figure 2. SEM images of the lateral surfaces of the fractured BMGs deformed at strain rates of 2×10^{-3}, and 2×10^{-4} s^{-1}, respectively.

It is well known that the jerky-flow behavior is actually a process of the strain energy accumulation and energy dissipation [19]. The elastic energy is accumulated during the stress rising, and a stress drop can be constructed to characterize the elastic energy during the relaxation process in each serration [15].

Recently, the SOC behavior exhibits in serrated flow with the variation of the elastic energy during the plastic deformation [14]. The SOC behavior is a self-similar or scale-free pattern [19], *i.e.*, the structures on one scale is almost the same with structures on the other scales. The transition of the plastic dynamics of the BMGs from a chaotic state finally to the SOC state is shown to correlate with different strain rates and temperatures [14]. To further investigate the SOC behavior of the serrated flows, the distribution of shear-avalanche sizes reflecting the shear avalanche in BMGs is discussed [27]. However, the shear avalanche size cannot be measured directly. In this case, the elastic energy density is selected to characterize the shear-avalanche sizes instead.

The strain-energy density of one serration event ($\Delta\delta$) is

$$\Delta\delta = \frac{1}{2}\Delta\sigma\Delta\varepsilon \tag{1}$$

where $\Delta\sigma$ and $\Delta\varepsilon$ are the elastic stress and strain in one serration event [28], as shown in Figure 1b. A normalization of the elastic energy density is applied to eliminate the statistical error, since the plastic strain causes a drift of the elastic energy density values [23]. The plots of the elastic energy density *versus* the strain are obtained at the strain rates of 2×10^{-3} and 2×10^{-4} s^{-1} with a baseline, $f(\varepsilon)$, through the linear-regression fitting, as shown in Figure 3a,c, respectively. The elastic energy density is linearly related with the variable quantity of the stress and strain. In Figure 3a, it is evident that the distribution of the elastic energy density is inhomogeneous, *i.e.*, the values of elastic energy density distribute with values lower than 7000 J/m^3 and higher than 10,000 J/m^3 at the strain rate of 2×10^{-3} s^{-1}. Compared with Figure 3a, most of the elastic energy densities in serrations are lower than 6000 J/m^3 at the strain rate of 2×10^{-4} s^{-1} in Figure 3c. Actually, it is interesting that many small amplitudes of serrations dominate at the strain rate of 2×10^{-4} s^{-1}. Once reaching the energy-accumulation limitation of some smaller amplitude serrations during the plastic deformation, the stored energy will be released quickly. Precisely owing to these small serrations, the amount of the low elastic energy density is larger than the other one, and the average amplitude of serrations is a little lower at different strain rates.

For sake of investigating the distribution of the normalized elastic energy density, a new non-dimensional variable $S = \Delta\delta/f(\varepsilon)$ is defined. The $f(\varepsilon)$ is a fitting function based on the strain (ε), which means the elastic energy density as well. If given a strain value, it is obtained a function value of elastic energy density by the fitting function $f(\varepsilon)$. Figure 3b,d are frequency distribution histograms, which display the $N(s)$ *versus* S, where $N(s)$ is the number of S. The stress drop generates shear bands, following a fractal structure [29], characteristic of a power-law relation, which indicates that shear banding may self-organize to a critical state, *i.e.*, the SOC behavior occurs [20,28]. From Figure 3b, it is obvious that the number of S reveals an increasing and then decreasing trends, which is similar to a normal distribution. The distribution of the elastic energy density is disordered, and the chaotic state appears in the serrated flows during the plastic deformation. In contrast, compared with Figure 3b, a clearly monotonical decreasing distribution is presented in Figure 3d, which is analogous to a power-law distribution. Moreover, the maximum value of S is 5.0, which is associated with the low values of the elastic energy density at lower strain, as shown in Figure 3c. Take the logarithm of S and $N(s)$, as displayed in the inset of Figure 3d. It is quite distinct that these scatters reveal a linear relation. In other words, the distribution of the elastic energy density exhibits a power-law distribution with

the power-law exponent, α, of −2.76, suggesting that the SOC behavior appears during serrated flows at the strain rate of 2×10^{-4} s^{-1}.

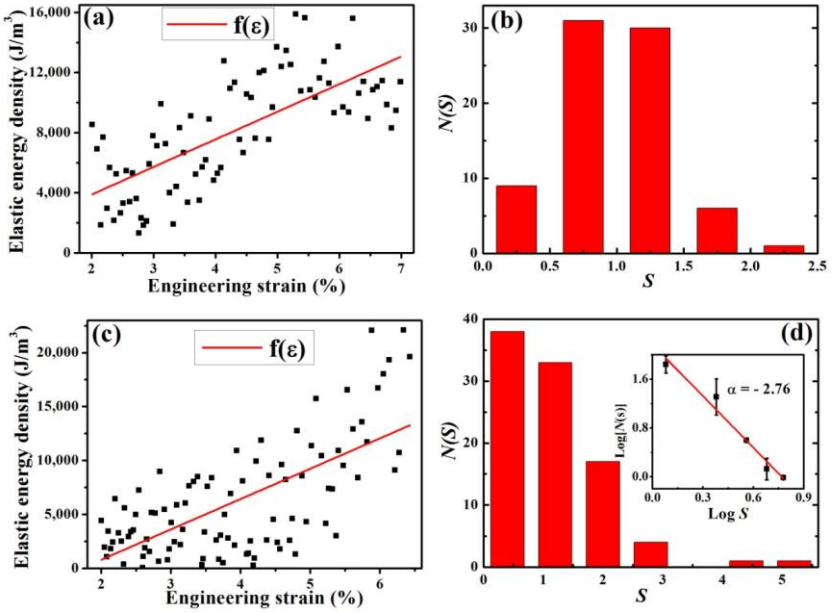

Figure 3. (**a**), (**c**) The profiles of elastic energy density *vs.* strain. The red lines are baselines, $f(\varepsilon)$, by linearly regression fitting at the strain rates of 2×10^{-3}, and 2×10^{-4} s^{-1}. (**b**), (**d**) The statistical distributions of elastic energy densities, $N(s)$ at the strain rates of 2×10^{-3}, and 2×10^{-4} s^{-1}, respectively. Inset shows a power-law distribution of the elastic energy density at the strain rate of 2×10^{-4} s^{-1}.

To further characterize the SOC behavior during serrated flows, the distribution of the cumulative probability of the elastic-energy density is investigated. The cumulative probability is the percentage of the number of serration events with the elastic energy density being larger than an elastic energy density, P ($\geq \Delta\delta$). The SOC behavior is in accordance with a power-law distribution function accompanied with a squared exponential decay function [19]:

$$P(\geq \Delta\delta) = A\Delta\delta^{-\beta}\exp\left[-\left(\frac{\Delta\delta}{\delta_C}\right)^2\right] \quad (2)$$

where A is a normalization constant, β is a scaling exponent, and δ_C the cut-off elastic energy density, which corresponds to the characteristic shearing size of the BMGs. The distributions of the cumulative probability of the elastic energy density at the strain rates of 2×10^{-3} and 2×10^{-4} s^{-1} are shown in Figure 4a,b, respectively. The larger elastic energy densities do not follow a power-law distribution, and decrease exponentially in probability [19]. It is quite evident that a perfect power-law distribution appears at the strain rate of 2×10^{-4} s^{-1} in Figure 4b, and the goodness of fit reaches 0.99. A general trend of power-law distribution with a goodness of fit of 0.95 is displayed in Figure 4a. Strictly speaking, it is not a power-law distribution but an intermediate state. Because there is no serrated flow at the strain rate of 2×10^{-2} s^{-1} and the serrated flow phenomenon occurs from the strain rate of 2×10^{-3} s^{-1}. Through the cumulative probability distribution analysis, the goodness of fit of the power-law function is as high as 0.95 at the strain rate of 2×10^{-3} s^{-1}. However, the goodness of fit

is 0.99 at the strain rate of 2×10^{-4} s^{-1}, which manifests the SOC behavior happens. In other words, the plastic dynamics of the BMGs is in an intermediate state, *i.e.*, the serrated flow takes place at the strain rate of 2×10^{-3} s^{-1} and when the strain rate changes, the SOC behavior occurs immediately. It is found that the structure disorder and the presence of defects cause the critical stresses at which slips initiate or stop to vary throughout the specimen and the extent of the power-law scaling regime is limited by the occurrence of large slip events [30]. Therefore, a power-law relation with an exponent of about 0.22 is obtained, which is manifested as the SOC behavior. The SOC state is a critical state at some strain rate and the characteristic value of the strain rate may be different due to composition or experiment condition, *etc.* For different compositions, the amplitudes of serrated flows, the stored energy in each serration are different, which lead to the changing of power-law distribution in statistical analysis. Therefore, the SOC state occurs with decreasing strain rates in current study. In other words, the transition of the plastic dynamics of the BMGs is from non-serrated flow to an intermediate state and finally to the SOC state with decreasing the strain rates.

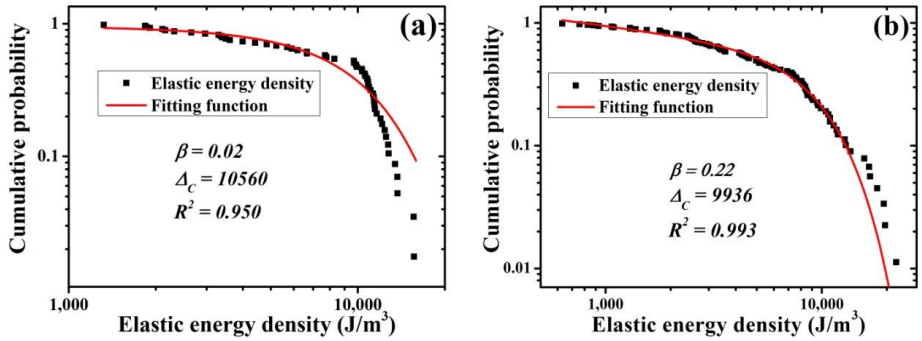

Figure 4. Cumulative probability distributions for the elastic energy density at the strain rates of 2×10^{-3}, and 2×10^{-4} s^{-1}, respectively. The red lines are fitted by Equation (2).

4. Conclusions

In summary, the statistical analysis of the distribution of the elastic energy density is very important to understand the serrated-flow behavior in BMGs. The yielding strengths of the Pd-based BMGs are almost the same values of 1650 MPa, and the compressive plasticities keep similar values about ~6% at different strain rates. The SOC behavior is observed at the strain rate of 2×10^{-4} s^{-1} during serrated flows. All the serrations with different strain rates are counted, and different dynamic statistical analyses are carried out. The serrated-flow behavior is not observed on the stress-strain curve at the strain rate of 2×10^{-2} s^{-1}. However, the medial state occurs at the strain rates of 2×10^{-3} s^{-1}, and eventually the SOC behavior appears at the strain rate of 2×10^{-4} s^{-1}. The distribution of the elastic energy density shows a power-law distribution with the power-law exponent of −2.76, suggesting that the SOC behavior appears, while the other distribution dose not exhibit a power-law distribution. In addition, the cumulative probability distribution of the elastic energy density is studied. The cumulative probability is well approximated by a power-law distribution function with the power-law exponent of 0.22 at the strain rate of 2×10^{-4} s^{-1}. The values of the goodness of fit are 0.95 and 0.99 at the strain rates of 2×10^{-3} and 2×10^{-4} s^{-1}, respectively. It is obvious that the dynamic serrated flow of BMGs

transform from non-serrated flow to an intermediate state and finally to the SOC state with decreasing the strain rates.

Acknowledgment

J.W.Q. would like to acknowledge the financial support of National Natural Science Foundation of China (No. 51371122), the Program for the Innovative Talents of Higher Learning Institutions of Shanxi (2013), and the Youth Natural Science Foundation of Shanxi Province, China (No. 2015021005).

Author Contributions

The statistical analysis was undertaken by Z.W., J.L. and J.Q. The microstructure analysis of the bulk metallic glass was performed by J.L. and B.W. The preparation of test samples was supported by Z.W. The paper was wrote by Z.W., J.Q. and B.W.

Conflicts of Interest

The authors declare no conflict of interest.

References

1. Axinte, E. Metallic glasses from "alchemy" to pure science: Present and future of design, processing and applications of glassy metals. *Mater. Des.* **2012**, *35*, 518–556.
2. Chen, M.W. Mechanical behavior of metallic glasses: Microscopic understanding of strength and ductility. *Annu. Rev. Mater. Res.* **2008**, *38*, 445–469.
3. Sun, B.A.; Pauly, S.; Hu, J.; Wang, W.H.; Kühn, U.; Eckert, J. Origin of intermittent plastic flow and instability of shear band sliding in bulk metallic glasses. *Phys. Rev. Lett.* **2013**, *110*, 225501.
4. Ke, H.B.; Sun, B.A.; Liu, C.T.; Yang, Y. Effect of size and base-element on the jerky-flow dynamics in metallic glass. *Acta Mater.* **2014**, *63*, 180–190.
5. Spaepen, F. A Microscopic mechanism for steady state inhomogeneous flow in metallic glasses. *Acta Metall*. **1977**, *25*, 407–415.
6. Argon, A.S. Plastic deformation in metallic glasses. *Acta Metall.* **1979**, *27*, 47–58.
7. Johnson, W.L.; Samwer, K. A Universal criterion for plastic yielding of metallic glasses with a $(T/T_g)^{2/3}$ temperature dependence. *Phys. Rev. Lett.* **2005**, *95*, 195501.
8. Lebyodkin, M.A.; Brechet, Y.; Estrin, Y.; Kubin, L.P. Statistics of the catastrophic slip events in the Portevin-Le Châtelier effect. *Phys. Rev. Lett*. **1995**, *74*, 4758–4761.
9. Argon, A.S. Strain avalanches in plasticity. *Philos. Mag.* **2013**, *93*, 3795–3808.
10. Kubin, L.P.; Ananthakrishna, G.; Fressengeas, C. Comment on "Portevin-Le Chatelier effect". *Phys. Rev. E* **2002**, *65*, 053501.
11. Ananthakrishna, G. Current theoretical approaches to collective behavior of dislocations. *Phys. Rep.* **2007**, *440*, 113–259.
12. Weiss, J.; Marsan, D. Three-dimensional mapping of dislocation avalanches: Clustering and space/time coupling. *Science* **2003**, *299*, 89–92.
13. Bak, P.; Tang, C.; Wiesenfeld, K. Self-organized criticality. *Phys. Rev. A* **1998**, *38*, 364–374.

14. Ren, J.L.; Chen, C.; Liu, Z.Y.; Li, R.; Wang, G. Plastic dynamics transition between chaotic and self-organized critical states in a glassy metal via a multi-fractal intermediate. *Phys. Rev. B* **2012**, *86*, 134303.
15. Qiao, J.W.; Zhang, Y.; Liaw, P.K. Serrated flow kinetics in a Zr-based bulk metallic glass. *Intermetallics* **2010**, *18*, 2057–2064.
16. Louzguine-Luzgin, D.V.; Zadorozhnyy, V.Y.; Chen, N.; Ketov, S.V. Evidence of the existence of two deformation stages in bulk metallic glasses. *J. Non-Cryst. Solids* **2014**, *396*, 20–24.
17. Qiao, J.W.; Jia, H.L.; Zhang, Y.; Liaw, P.K.; Li, L.F. Multi-step shear banding for bulk metallic glasses at ambient and cryogenic temperatures. *Mater. Chem. Phys.* **2012**, *136*, 75–79.
18. Klaümunzer, D.; Lazarev, A.; Maaß, R.; Dalla Torre, F.H.; Vinogradov, A.; Löffler, J.F. Probing shear-band initiation in metallic glasses. *Phys. Rev. Lett.* **2011**, *107*, 185502.
19. Wang, G.; Chan, K.C.; Xia, L.; Yu, P.; Shen, J.; Wang, W.H. Self-organized intermittent plastic flow in bulk metallic glasses. *Acta Mater.* **2009**, *57*, 6146–6155.
20. Sun, B.A.; Yu, H.B.; Jiao, W.; Bai, H.Y.; Zhao, D.Q.; Wang, W.H. Plasticity of ductile metallic glasses: A self-organized critical state. *Phys. Rev. Lett.* **2010**, *105*, 035501.
21. Zhang, W.; Guo, H.; Li, Y.H.; Wang, Y.M.; Wang, H.; Chen, M.W.; Yamaura, S. Formation and properties of P-free Pd-free metallic glasses with high glass-forming ability. *J. Alloys Compd.* **2014**, *67*, 310–313.
22. Qiao, J.W.; Wang, Z.; Yang, H.J.; Li, M.; Liang, W.; Xu, B.S. Exponential decay of shearing stress during jerky flows in a Zr-based bulk metallic glass. *AIP Adv.* **2013**, *3*, 032105.
23. Sun, B.A.; Pauly, S.; Tan, J.; Stoica, M.; Wang, W.H.; Kühn, U.; Eckert, J. Serrated flow and stick-slip deformation dynamics in the presence of shear-band interactions for a Zr-based metallic glass. *Acta Mater.* **2012**, *60*, 4160–4171.
24. Antonaglia, J.; Xie, X.; Schwarz, G.; Wraith, M.; Qiao, J.W.; Zhang, Y.; Liaw, P.K.; Uhl, J.T.; Dahmen, K.A. Tuned critical avalanche scaling in bulk metallic glasses. *Sci. Rep.* **2014**, *4*, 4382.
25. Wang, Z.; Qiao, J.W.; Yang, H.J.; Liaw, P.K.; Huang, C.J.; Li, L.F. Serration dynamics in a Zr-based bulk metallic glass. *Metall. Mater. Trans. A* **2015**, *46*, 2404–2414.
26. Qiao, J.W.; Wang, Z.; Jiao, Z.M.; Yang, H.J.; Ma, S.G.; Wang, Z.H.; Xu, B.S. Predicting burst sizes in amorphous alloys during plastic flows. *Mater. Sci. Eng. A* **2014**, *609*, 222–225.
27. Richeton, T.; Weiss, J.; Louchet, F. Breakdown of avalanche critical behavior in polycrystalline plasticity. *Nat. Mater.* **2005**, *4*, 465–469.
28. Ren, J.L.; Chen, C.; Wang, G.; Mattern, N.; Eckert, J. Dynamics of serrated flow in a bulk metallic glass. *AIP Adv.* **2011**, *1*, 032158.
29. Sun, B.A.; Wang, W.H. Fractal nature of multiple shear bands in severely deformed metallic glass. *Appl. Phys. Lett.* **2011**, *98*, 201902.
30. Antonaglia, J.; Wright, W.J.; Gu, X.J.; Byer, R.R.; Hufnagel, T.C.; LeBlanc, M.; Uhl, J.T.; Dahmen, K.A. Bulk metallic glasses deform via slip avalanches. *Phy. Rev. Lett.* **2014**, *112*, 155501.